Magnetic phase diagram of the stage-1 $CoCl_2$ graphite intercalation compound: Existence of metamagnetic transition and spin-flop transitions

Itsuko S. Suzuki,* Ting-Yu Huang, and Masatsugu Suzuki†
Department of Physics, State University of New York at Binghamton, Binghamton, New York 13902-6016
(Received 17 January 2002; revised manuscript received 10 April 2002; published 13 June 2002)

The H-T phase diagram of a stage-1 $CoCl_2$ graphite intercalation compound has been determined from measurements of the ac magnetic susceptibility, dc magnetization, and in-plane resistivity in the presence of an external magnetic field along the c plane perpendicular to the c axis. This compound undergoes two magnetic phase transitions at T_{cu} $(=T_N=9.9$ K) and T_{cl} $(=7.7$ K) at $H=0$. A metamagnetic transition occurs at a critical point ($T_3\approx 8.77$ K, $H_3\approx 270$ Oe). A spin-flop transition occurs at the critical point ($T_2\approx 6.8$ K, $H_2\approx 80$ Oe) due to a competition between weak antiferromagnetic interplanar interactions and in-plane anisotropic interactions. Two lines H_+ and H_- above T_N are due to ferromagnetic short-range fluctuations.

DOI: 10.1103/PhysRevB.65.224432 PACS number(s): 75.30.Kz, 75.40.Cx, 75.50.Ee

I. INTRODUCTION

A stage-1 $CoCl_2$ graphite intercalation compound (GIC) magnetically behaves like a quasi-two-dimensional (2D) ferromagnet with a weak antiferromagnetic interplanar exchange interaction. The spin easy direction of Co^{2+} lies in the c plane, showing an easy-plane (XY) type anisotropy. The magnetic phase transition of a stage-1 $CoCl_2$ GIC has been extensively studied using magnetic neutron scattering, dc and ac magnetic susceptibility, magnetization, and in-plane and c-axis resistivity.[1–7] It has been revealed through these studies that this compound undergoes an antiferromagnetic phase transition at a Néel temperature T_N $(=9.9$ K). Below T_N the 2D ferromagnetic $CoCl_2$ layers are antiferromagnetically stacked along the c axis, forming a 3D antiferromagnetic long-range order. In fact, Ikeda *et al.*[5] measured magnetic neutron-scattering intensities of a stage-1 $CoCl_2$ GIC, and showed that relatively sharp antiferromagnetic Bragg reflections appear at wave numbers $Q_c=(2\pi/I_c)L$, with $L=\frac{1}{2}$, $\frac{3}{2}$, and so on, where I_c is the c-axis repeat distance. The Bragg intensity at $(00\frac{1}{2})$ decreases as the temperature (T) increases, and tends to reduce to zero, indicating a 3D antiferromagnetic ordered below T_N. The transition is somewhat smeared probably because of the islandlike nature of this compound. The spin correlation length along the c axis, ξ_c, is limited to be over about 20 $CoCl_2$ layers ($\approx$200 Å). Note that in a stage-1 $CoCl_2$ GIC, the $CoCl_2$ layers are formed of small islands, which is common to acceptor-type GIC's. The peripheries of islands provide acceptor sites for electrons transferred from the graphite layer to the $CoCl_2$ layer.[3]

The magnetic phase diagram of a stage-1 $CoCl_2$ GIC was studied by Nicholls and Dresselhaus.[3] They measured the field dependence of the dispersion χ' of ac magnetic susceptibility when an external magnetic field (H) is applied along the c plane (perpendicular to the c axis). They showed that the H dependence of χ' exhibits a peak at a characteristic magnetic field ($H_t\approx 380$ Oe) at low temperatures. As T is raised, this peak becomes sharper and stronger in magnitude and then disappears around 10 K just above T_N. They suggested two possible interpretations for the behavior. In the first interpretation, H_t is a spin-flop transition field. This possibility is ruled out because the spin flop to paramagnetic transition at higher H has not been detected up to a field of 10 kOe. In the second interpretation, H_t is a metamagnetic transition field. They concluded that the metamagnetic transition is more likely in a stage-1 $CoCl_2$ GIC. The nature of the field-induced transition was also examined from magnetic neutron scattering by Chouteau *et al.*[6] The intensity of antiferromagnetic Bragg reflection at $(00\frac{1}{2})$ starts to decrease at $\approx$400 Oe, and seems to disappear at $\approx$800 Oe at 1.7 K.

In spite of such success, so far the complicated T dependence of ac magnetic susceptibility near T_N is not fully understood in terms of the above simple model. In fact, Nicholls and Dresselhaus[3] showed that χ' has two peaks at 9.7 and 8.6 K, and that the absorption χ'' has a single peak at 9.7 K. Yazami and Chouteau[4] showed that χ' has a peak at 9.77 K and a shoulder at 8.22 K, and that χ'' has two peaks at 9.77 and 8.22 K. These results suggest that an ordered phase may exist below T_N.

In this paper we have determined the H-T phase diagram of a stage-1 $CoCl_2$ GIC precisely using superconducting quantum interference device (SQUID) ac magnetic susceptibility and SQUID dc magnetization, and in-plane resistivity in the presence of an external magnetic field H along the c plane. The H-T diagram thus obtained is much more complicated than we expected. The antiferromagnetic phase transition occurs at an upper critical temperature T_{cu} $(=T_N=9.9$ K). A metamagnetic transition is observed at a critical point ($T_3\approx 8.77$ K and $H_3\approx 270$ Oe). Spin-flop transitions are newly observed at points ($T_1\approx 7.6$ K, $H_1\approx 8$ Oe) and ($T_2\approx 6.8$ K, $H_2\approx 80$ Oe) below a lower critical temperature T_{cl} $(=7.7$ K). These results indicate that the ordered phases below T_N have several different spin structures depending on T and H. The H-T diagram of a stage-1 $CoCl_2$ GIC will be discussed in comparison with those of Ising antiferromagnets $FeCl_2$ (Refs. 8 and 9) and $FeBr_2$,[10–14] showing metamagnetic transitions. In $FeCl_2$ and $FeBr_2$, the 2D ferromagnetic layers are antiferromagnetically stacked along the c axis, forming a 3D antiferromagnetic phase below the Néel temperature. In spite of such similarities, the magnetic phase diagram of $FeBr_2$ is much more complicated than that of $FeCl_2$. The present study is motivated by a series of works on $FeBr_2$.[10–14]

II. PRELIMINARY DETAILS

In a stage-1 $CoCl_2$ GIC, there is a single graphite layer between adjacent $CoCl_2$ layers. The *c*-axis repeat distance is 9.38 Å. The structure of the $CoCl_2$ layer consists of Co^{2+} layers which are sandwiched between two Cl^- layers along the *c* axis. The Co layers are formed of a triangular lattice with an in-plane lattice constant $a=3.572$ Å.[15] The spin Hamiltonian of stage-1 and stage-2 $CoCl_2$ GIC's is written as

$$H=-2J\sum_{\langle i,j\rangle}\mathbf{S}_i\cdot\mathbf{S}_j+2J_A\sum_{\langle i,j\rangle}S_i^z\cdot S_j^z+2J'\sum_{\langle i,k\rangle}\mathbf{S}_i\cdot\mathbf{S}_k,\quad(1)$$

with a fictitious spin $S=1/2$, where J is the ferromagnetic intraplanar exchange interaction between the nearest-neighbor Co^{2+} pairs (i,j) in the same Co layer, J_A is the anisotropic exchange interaction favoring XY anisotropy, and $(-J')$ is the antiferromagnetic interplanar exchange interaction between the nearest-neighbor Co^{2+} pairs (i,k) in the adjacent Co layers. The values of J and J_A are assumed to be the same for stage-1 and stage-2 $CoCl_2$ GIC's ($J=7.75$ K and $J_A=3.72$ K), while the value of J' for stage-1 $CoCl_2$ is much larger than that for a stage-2 $CoCl_2$ GIC.[1,16] For convenience, we introduce the equivalent fields (intraplanar exchange field, interplanar exchange field, and XY anisotropy field) defined by

$$H_E=\frac{2zJS}{g_a\mu_B},\quad H_E'=\frac{2z'J'S}{g_a\mu_B},\quad H_A^{out}=\frac{2zJ_AS}{g_c\mu_B},\qquad(2)$$

respectively, where g_a (=6.40) and g_c (=4.75) are the Landé g factors along the c plane and along the c axis, respectively, z (=6) is the number of in-plane nearest-neighbor Co atoms, and z' (= 6) is the number of in-plane nearest-neighbor Co atoms. The values of H_E and H_A^{out} are estimated as 108.3 and 70 kOe, respectively. The value of H_E' is on the order of 380 Oe for a stage-1 $CoCl_2$ GIC (see Sec. VI). Note that an in-plane sixfold symmetry-breaking field H_A^{in} is not included in the above spin Hamiltonian. The value of H_A^{in} is on the order of 10 Oe (see Sec. VI). Because of H_A^{in}, the direction of spin in the c plane is limited to the angle given by $\phi=(\pi/6)n$ $(n=0,1,\ldots,5)$, where ϕ is the angle between the spin and an in-plane crystalline axis.[2,17] The competitions between H_A^{in} and H_E' and between H_E' and H_A^{out} lead to the occurrence of the spin-flop transition and the metamagnetic transition, respectively.

III. MOLECULAR FIELD THEORY

Here we present a simple model of the molecular field theory for the spin-flop transition and metamagnetic transition.[18,19] For simplicity, we consider an antiferromagnetic system where the sublattice magnetizations ($\mathbf{M}_1$ and $\mathbf{M}_2$) are collinear with the easy axis (z axis) at $H=0$. When $\mathbf{H}$ is applied along the z axis, the direction of the sublattice magnetizations may rotate in the (x,z) plane. When the sublattice magnetizations are parallel to the z axis, the free energy of the system is given by $F_\parallel=-\chi_\parallel H^2/2-K$, where $\chi_\parallel$ is the susceptibility along the z axis and K is the anisotropy energy. On the other hand, when the sublattice magnetizations lie in the (x,z) plane, the free energy is given by $F_\perp=-\chi_\perp' H^2/2$, where $\chi_\perp'$ is the susceptibility along the z axis. The susceptibility $\chi_\perp'$ is not the same as $\chi_\perp$ which is the susceptibility along the x axis when $\mathbf{H}$ is applied along the x axis. At a critical field H_{SF} defined by

$$H_{SF}=[2K/(\chi_\perp'-\chi_\parallel)]^{1/2},\qquad(3)$$

the free energy of the two states are equal $(F_\parallel=F_\perp)$. Hence, for $H<H_{SF}$, the sublattice magnetizations are parallel to the z axis, whereas for $H>H_{SF}$ the sublattice magnetizations lie in the (x,z) plane. The change for the parallel to the perpendicular orientation is called spin flopping. At $T=0$ K, we have $\chi_\parallel=0$ from the definition. The susceptibility $\chi_\perp'$ can be derived as follows. To this end we define the exchange fields $\mathbf{H}_E^{(1)}=-A\mathbf{M}_2$ and $\mathbf{H}_E^{(2)}=-A\mathbf{M}_1$ where $|\mathbf{M}_1|=|\mathbf{M}_2|=M$, A is constant, and $|\mathbf{H}_E^{(i)}|=H_E^0=AM$. We also define the anisotropic field $\mathbf{H}_A^{(i)}=(KM_{iz}/M^2)\hat{z}$ $(i=1,2)$ which is directed along the z axis. When θ is the angle between $\mathbf{M}_1$ and the x axis, the anisotropic field is expressed by $\mathbf{H}_A^{(i)}=H_A^0\sin\theta\hat{z}$ with $H_A^0=K/M$. The condition that the resultant magnetic field $(\mathbf{H}+\mathbf{H}_A^{(i)}+\mathbf{H}_E^{(i)})$ should be parallel to $\mathbf{M}_i$ leads to a relation

$$\tan\theta=\frac{H+H_A^0\sin\theta-H_E^0\sin\theta}{H_E^0\cos\theta}\quad\text{or}\quad\sin\theta=\frac{H}{2H_E^0-H_A^0}.\qquad(4)$$

Then $\chi_\perp'$ can be obtained as $\chi_\perp'=(M_{1z}+M_{2z})/H=2M\sin\theta/H=2M/(2H_E^0-H_A^0)=1/[A-K/(2M^2)]$. Using this relation for $\chi_\perp'$ in Eq. (3), the spin flop field H_{SF} can be expressed by $H_{SF}=[H_A^0(2H_E^0-H_A^0)]^{1/2}$. The magnetic field H_s at which the net magnetization saturates is defined by Eq. (4) with $\theta=\pi/2$: $H_s=2H_E^0-H_A^0$. Since $H_S^2-H_{SF}^2=2(2H_E^0-H_A^0)(H_E^0-H_A^0)$, the inequality $H_{SF}<H_S$ holds valid only for $H_E^0>H_A^0$. For $H_E^0<H_A^0$, the metamagnetic transition occurs from the antiferromagnetic state to the ferromagnetic state at $H=H_E^0$, where $F_{AF}=F_F$. The free energy of the system is described by $F_{AF}=-AM^2$ for the antiferromagnetic state and by $F_F=AM^2-2HM$ for the ferromagnetic state.

For the spin-flop transition, the H-T diagram consists of an antiferromagnetic (AF) phase, a spin-flop (SF) phase, and a paramagnetic (P) phase [see Fig. 1(a)]. The boundary between the AF and SF phases is a first-order transition line, while the boundaries between the SF and P phases and between the AF and P phases are second-order transition lines. These three boundaries meet a critical point. For the metamagnetic transition, the H-T diagram consists of an AF phase and a P phase [see Fig. 1(b)]. The boundary between the AF and P phases is perfectly smooth at a critical point. The boundary at the high-T side above the critical point is a second-order transition line, while the boundary at the low-T side below the critical point is a first-order transition line.

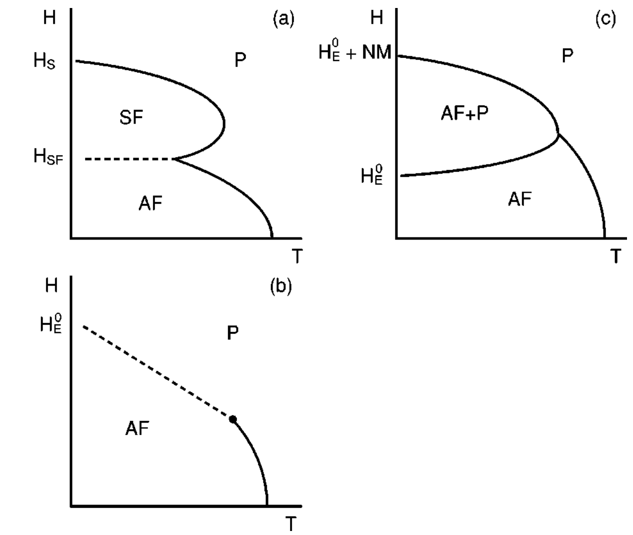

FIG. 1. (a) Schematic H-T diagram for the spin-flop transition ($H_E^0 > H_A^0$). The second-order critical lines (P-AF, P-SF) (solid lines) meet the first-order spin-flop line (the dotted line) tangentially at a multicritical point. $H_s = 2H_E^0 - H_A^0$ and $H_{SF} = [H_A^0(2H_E^0 - H_A^0)]^{1/2}$. (b) Schematic H-T diagram for metamagnetic transition ($H_E^0 < H_A^0$). The second-order critical line (the solid line) meets the first-order line (the dotted line) at a critical point. (c) Experimental observation of a metamgnetic transition. H is an external magnetic field and H_i is an internal field defined by Eq. (5). The demagnetizing effect opens the coexistence line (P-AF) into a coexistence area of the AF phase and P phase [(AF+P) phase]. See the details in Sec. VI B.

Figure 1(c) shows the schematic H-T diagram for the metamagnetic transition experimentally observed. The applied field H is different from the internal field H_i by

$$H_i = H - NM(H_i), \tag{5}$$

where N is the demagnetizing factor of the system and $M(H_i)$ is the magnetization as a function of H_i. See the detail of the H-T diagram in Sec. VI B. Typical examples of a spin-flop transition and a metamagnetic transition were reported for MnF_2 (Ref. 20) and $FeCl_2$,[8,9] respectively.

IV. EXPERIMENTAL PROCEDURE

We used a sample of a stage-1 $CoCl_2$ GIC with a stoichiometry of $C_{5.63}CoCl_2$. The density of this system is calculated as $\rho_m = 2.06$ g/cm^3. The dimension of the sample used for the magnetic measurements was 3×4 mm^2 in the c plane and 0.2 mm in thickness along the c axis. The ac magnetic susceptibility and DC magnetization were measured using a SQUID magnetometer (Quantum Design, MPMS XL-5) with an ultra-low-field capability as an option. A field-cooled magnetization (M_{FC}) was measured with decreasing T from 25 to 1.9 K with H, where the sample was annealed for 10 min at 30 K in the presence of H along the c plane before measurement. The H dependence of zero-field-cooled magnetization (M_{ZFC}) at fixed T was measured with increasing H from 0 to 1 kOe, where the sample was cooled from 298 K to T at $H = 0$ before the measurement. The dispersion (χ') and absorption (χ'') were measured with increasing T from 1.9 to 18 K in the presence of H ($0 \leq H \leq 10$ kOe), where the frequency of the ac field was $f = 1$ Hz and the amplitude of the ac field was $h = 50$ mOe.

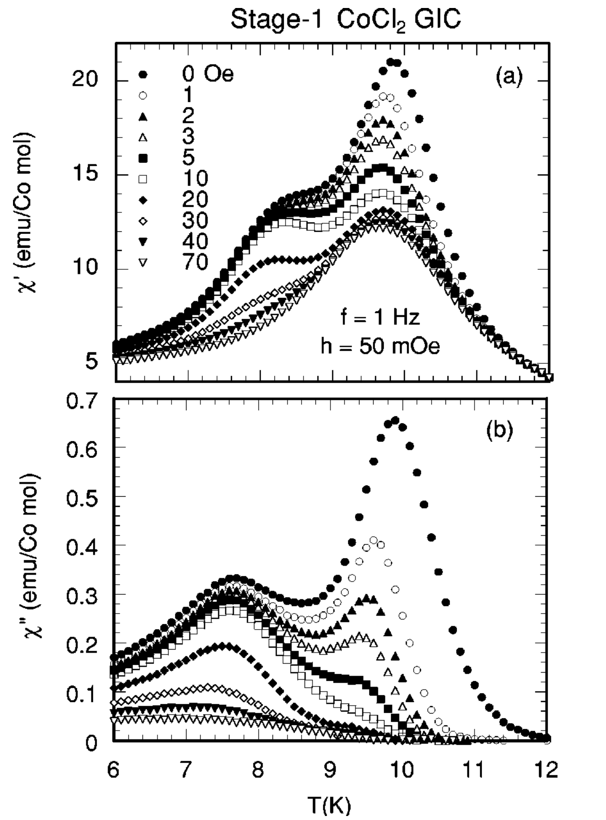

FIG. 2. T dependence of (a) χ' and (b) χ'' for a stage-1 $CoCl_2$ GIC ($0 \leq H \leq 70$ Oe). $h = 50$ mOe. $f = 1$ Hz. $H \perp c$ (c is the c axis). $h \perp c$.

The in-plane resistivity ρ was measured by a conventional four-probe method using an external device control option of the SQUID magnetometer. Two pairs of gold wires as the current and voltage probes were attached to the sample by silver paste (4922N, du Pont). The current was supplied through the current probes by a Keithley type 224, programmable dc current source. The voltage generated across the voltage probes was measured by a Keithley 182 nanovoltmeter. The measurements of ρ were made with increasing T from 1.9 to 20 K and then with decreasing T from 20 to 1.9 K in the presence of H ($0 \leq H \leq 10$ kOe) along the c plane.

V. RESULT

We have measured the T dependence of χ' and χ'' at $H = 0$ for a stage-1 $CoCl_2$ GIC, where $h = 50$ mOe and frequency f is varied between 0.01 and 1000 Hz. The dispersion χ' has a peak at 9.85 K independent of f, and a shoulder around 8 K. The absorption χ'' has a sharp peak at 9.9 K independent of f, and a broad peak at 7.59 K at $f = 0.01$ Hz. This broad peak in χ'' shifts to the high T side with increasing f: 8.0 K at $f = 1$ kHz. Figures 2–4 show the T dependence of χ' and χ'' for a stage-1 $CoCl_2$ GIC in the presence of H along the c plane, where $h = 50$ mOe and f

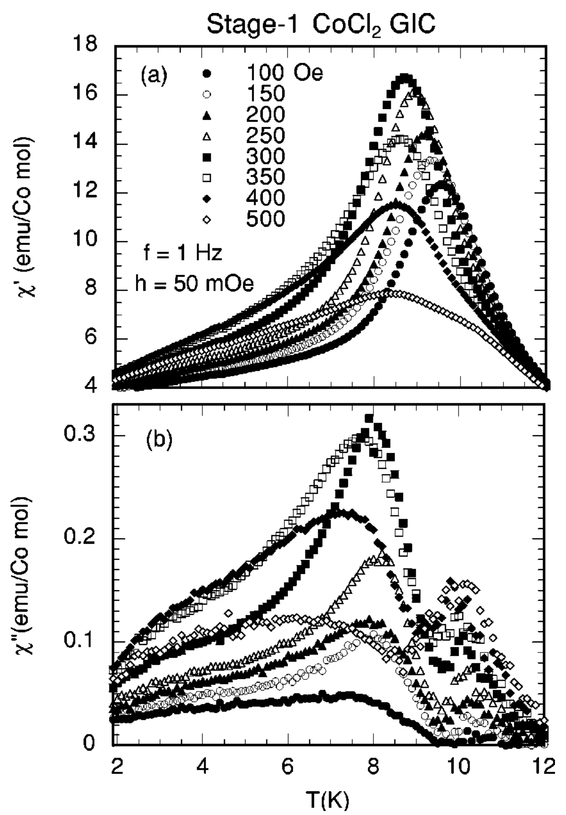

FIG. 3. T dependence of (a) χ' and (b) χ'' for a stage-1 $CoCl_2$ GIC ($100 \leqslant H \leqslant 500$ Oe). $h = 50$ mOe. $f = 1$ Hz. $H \perp c$. $h \perp c$.

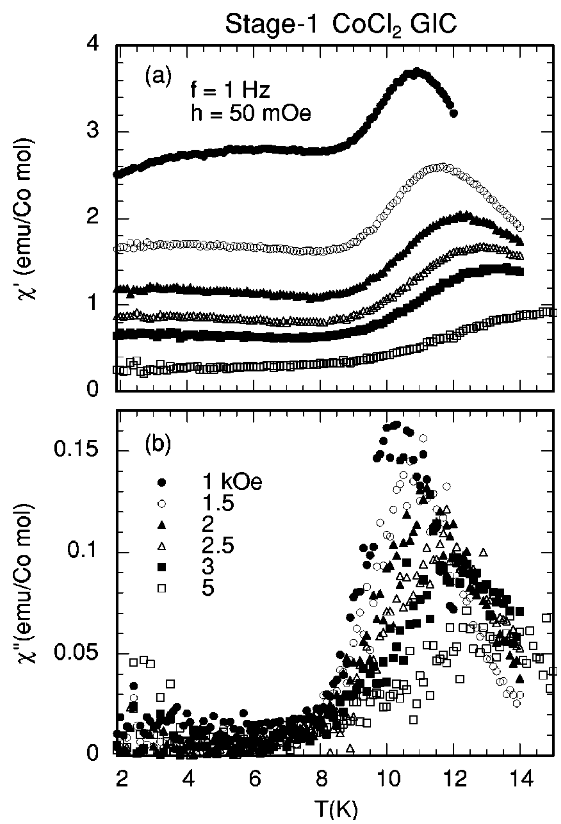

FIG. 4. T dependence of (a) χ' and (b) χ'' for a stage-1 $CoCl_2$ GIC ($1 \leqslant H \leqslant 5$ kOe). $h = 50$ mOe. $f = 1$ Hz. $H \perp c$. $h \perp c$.

$=1$ Hz. The absorption χ'' has two peaks at 9.9 and 7.7 K at $H=0$. For convenience hereafter these peak temperatures of χ'' are defined as an upper critical temperature T_{cu} ($=T_N = 9.9$ K) and a lower critical temperature T_{cl} ($=7.7$ K), respectively. Note that the peak temperature ($T_N = 9.9$ K) at $H=0$ shifts to 9.7 K even at $H=1$ Oe. Such a drastic shift of T_{cu} with H may be related to the symmetry breaking of XY anisotropy, but is not well understood at present. The peak height of χ'' at $H=0$ drastically decreases with increasing H. This peak becomes a shoulder above 6 Oe and disappears above 40 Oe. The peak at T_{cl} becomes broader with increasing H and disappears above 700 Oe. Another peak appears at T higher than 10.5 K above 100 Oe, shifting to the high-T side with further increasing H.

In contrast, the dispersion χ' has a peak at 9.85 K close to T_N and a broad shoulder around 8.5 K at $H=0$. The peak at 9.85 K shifts to the low-T side with increasing H (down to 3.1 K at $H=2$ kOe). The shoulder around 8.5 K changes into a peak only for $5 \leqslant H \leqslant 20$ Oe. Another peak appears at T higher than 10.15 K above 700 Oe, shifting to the high-T side with further increasing H.

Figure 5(a) shows the T dependence of the field-cooled (FC) magnetization M_{FC} along the c plane. The magnetization M_{FC} was measured with decreasing T from 20 to 1.9 K in the presence of H along the c plane. The magnetization M_{FC} shows a peak around T_N for $H \leqslant 300$ Oe, but it increases with decreasing T for $H \geqslant 400$ Oe. Figure 5(b) shows the T dependence of dM_{FC}/dT for various H's. At $H = 5$ Oe, dM_{FC}/dT has two local minima at 8.48 and 10.01 K, and a local maximum at 9.20 K. This local maximum shifts to the low T side with increasing H and disappears above 300 Oe.

Figure 6(a) shows the H dependence of the zero-field-cooled (ZFC) magnetization M_{ZFC} along the c plane at fixed T. First the sample was cooled from 298 K to T at $H=0$. Then M_{ZFC} at T was measured with increasing H from 0 to 1 kOe. In Fig. 6(b) we show the H dependence of dM_{ZFC}/dH at each T, which is obtained from Fig. 6(a). The derivative dM_{ZFC}/dH for $T=4.5$ K shows a sharp peak at a low field $H_l = 15$ Oe and a broad peak at a high field $H_u = 375$ Oe. The value of H_u is almost the same as that of the peak field of $\chi'(H)$ reported by Nicholls and Dresselhaus.[3] The lower field H_l decreases with increasing T and reduces to zero around T_{cl}. In contrast, the higher field H_u decreases with increasing T and reaches 300 Oe at 8.5 K. It tends to reduce to zero around T_N.

Figure 7(a) shows the T dependence of the normalized in-plane resistivity ρ/ρ_0 for a stage-1 $CoCl_2$ GIC at various H's along the c plane, where ρ_0 is the in-plane resistivity at $H=2$ kOe and $T=2K$. The in-plane resistivity in the presence of H is measured with increasing T from 1.9 to 20 K [$\rho(T\uparrow)$] and with decreasing T from 20 to 1.9 K [$\rho(T\downarrow)$]. We note that the value of $\rho(T\downarrow)$ is smaller than $\rho(T\uparrow)$ below a characteristic temperature T_0 for $350 < H < 700$ Oe, showing an irreversible effect of in-plane resistivity. The value of T_0 is dependent on H. Figure 7(b) shows the T dependence of $d(\rho/\rho_0)/dT$. The T derivative $d(\rho/\rho_0)/dT$ shows a local minimum at 9.4 K at $H=0$. This negative peak shifts

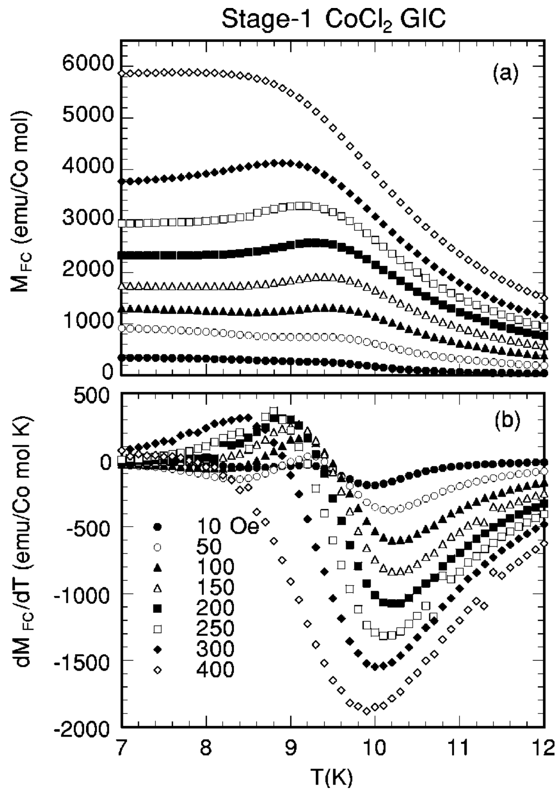

FIG. 5. T dependence of (a) M_{FC} and (b) dM_{FC}/dT at various H's for a stage-1 $CoCl_2$ GIC. $H \perp c$.

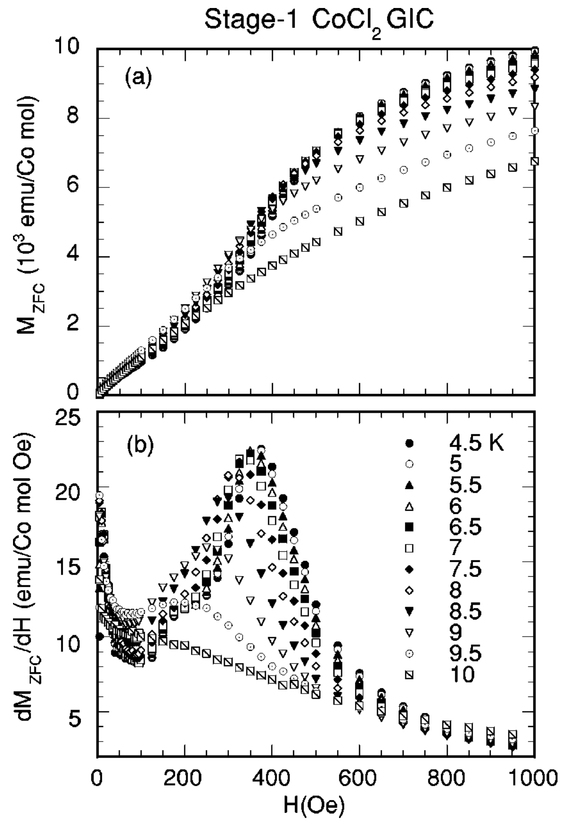

FIG. 6. H dependence of (a) M_{ZFC} and (b) dM_{ZFC}/dH at various T's for a stage-1 $CoCl_2$ GIC. $H \perp c$.

to the low-T side with increasing H, and disappears above 650 Oe.

VI. DISCUSSION

A. Overview of the H-T diagram

We have determined the H-T diagram of a stage-1 $CoCl_2$ GIC. Figure 8 shows the overall H-T diagram of a stage-1 $CoCl_2$ GIC. Since the antiferromagnetic interplanar exchange interaction is very weak, the entire phase diagram is accessible below 2 kOe. Figures 9(a)–9(d) show simplified H-T diagrams for several regions in the (T,H) plane. In Figs. 8 and 9 the peak temperatures for χ' vs T and χ'' vs T with $f=1$ Hz and $h=50$ mOe are denoted by open and closed circles for each H, respectively. The peak field of dM_{ZFC}/dH vs H are denoted by open squares for each T. The local-maximum and local-minimum temperatures of dM_{FC}/dT vs T are denoted by closed triangles for each H, respectively. The local-minimum temperatures of $d(\rho/\rho_0)/dT$ vs T are denoted by crosses. In Fig. 9(a), for comparison, we also show the H-T diagram obtained by Nicholls and Dresselhaus,[3] where the peak field of χ' vs H is denoted by open diamonds for each T. We note that the peak field of $\chi'(H)$ is in good agreement with that of dM_{ZFC}/dH vs H.

For convenience, the phase boundaries are denoted by the lines H_{ci} $(i=1-7)$, H_c, H_+, H_-. The nature of these lines will be discussed in Secs. VI B and VI C. The features of the H-T diagram shown in Figs. 8 and 9 are summarized as follows. (i) A metamagnetic transition occurs at a critical point $(T_3=8.77$ K, $H_3=270$ Oe$)$, which is the intersection of the lines H_{c4}, H_{c5}, H_{c7}, and H_c. The lines H_{c4} and H_{c5} denote the phase boundaries from the AF phase to the P phase via a mixed phase (AF+P). The region above the boundary H_{c5} is the P phase: $H_{c5}\approx 1.7$ kOe at 3.3 K. (ii) The line H_c connecting between the two points $[(T_N, H=0)$ and $(T_3, H_3)]$ is a second-order line. (iii) The line H_{c5} smoothly joins to the line H_{c7} at the critical point (T_3, H_3). The line H_{c7} intersects with the T axis at T_N' $(=9.25$ K) below T_N. (iv) The local minimum of $d(\rho/\rho_0)/dT$ occurs only near the lines H_{c7} and H_{c5}. (v) At high temperatures above T_N there are two lines denoted by H_+ and H_-: $H_+=7$ kOe at 16.56 K and $H_-=10$ kOe at 15.45 K. Line H_- seems to originate from a point $(T_N, H=0)$. The origin of lines H_+ and H_- is due to ferromagnetic short-range fluctuations which is noncritical. Similar lines are observed in the paramagnetic region of (T,H) plane in $FeBr_2$.[10–14] The discussion on these lines was given in Ref. 10. (vi) A spin-flop transition occurs at a critical point $(T_1\approx 7.6$ K, $H_1\approx 7$ Oe$)$ [see the inset of Fig. 9(c)], which is the intersection of the lines H_{c1} and H_{c2}. (vii) A spin-flop transition occurs at a critical point $(T_2\approx 6.8$ K, $H_2\approx 80$ Oe$)$, which is the intersection of the lines H_{c2} and H_{c3} [see Fig. 9(a)]. (viii) A spin-flop transition may occur at a critical point $(T_4\approx 9.3$ K, $H_4\approx 7$ Oe$)$ [see Fig. 9(d)].

B. Spin-flop transition and metamagnetic transition

We discuss the nature of the spin-flop transition at the critical point (T_2, H_2) and the metamagnetic transition at the

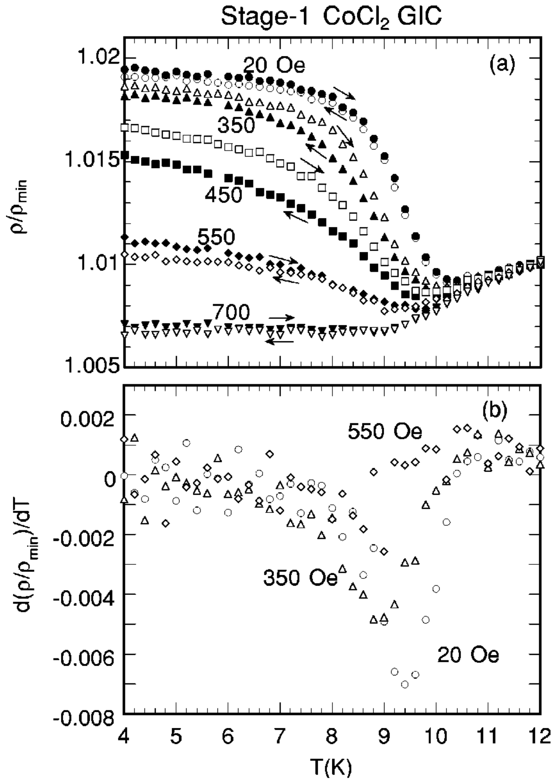

FIG. 7. T dependence of normalized in-plane resistivity ρ/ρ_0 for a stage-1 $CoCl_2$ GIC for various H's, which is measured with increasing T and decreasing T between 1.9 and 20 K. ρ_0 is the in-plane resistivity at $H=2$ kOe and $T=2$ K. $H\perp c$. (b) T dependence of $d(\rho/\rho_0)/dT$ for various H's, where ρ is obtained from the measurement with decreasing T.

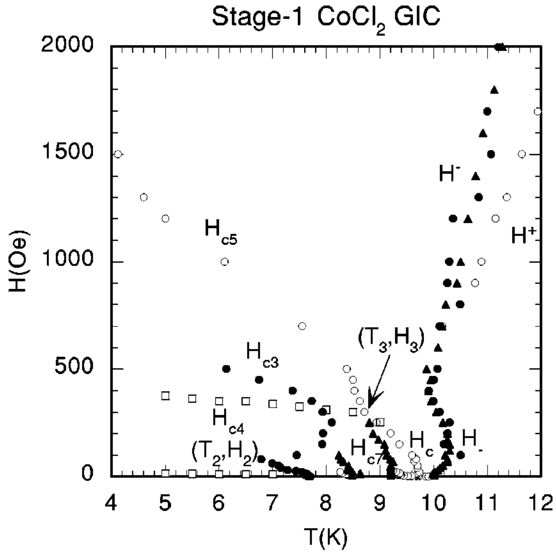

FIG. 8. Overview of the H-T diagram for a stage-1 $CoCl_2$ GIC, which is determined from the T dependence of χ' (○), χ'' (●), and dM_{FC}/dT (▲), and the H dependence of dM_{ZFC}/dH (□). H ($\perp c$, c is the c axis) is the value of external field. Lines H_c, H_{c3}, H_{c4}, H_{c5}, and H_{c7} are the phase boundaries. The coordinates (T_3, H_3) and (T_2, H_2) are critical points. Lines H_- and H_+ are due to ferromagnetic short-range fluctuations.

critical point (T_3, H_3) [see Fig. 9(a)]. In a stage-1 $CoCl_2$ GIC, three competing fields H_A^{in}, H_E', and H_A^{out} contribute to the field-induced transitions. Since $H\ll H_A^{out}$, the direction of spins along the c axis is energetically unfavorable. In this sense the field transitions have a XY character. As described in Sec. III, the competition between two fields $H_E^0=H_E'$ and $H_A^0=H_A^{in}$ ($H_E'\gg H_A^{in}$) leads to a spin-flop transition at the critical point (T_2, H_2) [see Fig. 1(a)]. The spin-flop transition between the AF and SF phases is of first order. Line H_{c2} meets line H_{c3} tangentially at the critical point (T_2, H_2). Note that the boundary between the SF and AF phases is not observed in the present work, partly because of the first-order transition. The spin-flop field at $T=0$ K can be described by

$$H_2=[(2H_E'-H_A^{in})H_A^{in}]^{1/2}\approx(2H_E'H_A^{in})^{1/2}. \qquad (6)$$

The transition between the SF and P phases, which is of second order, occurs on the line H_{c3}: $H_{c3}=2H_E'-H_A^{in}\approx 2H_E'$. In Fig. 9(a) we find $H_2=80$ Oe at $T_2=6.8$ K and $H_{c3}=500$ Oe at $T=6.14$ K.

In contrast, the competition between two fields $H_E^0=H_E'$ and $H_A^0=H_A^{out}$ ($H_E'\ll H_A^{out}$) leads to the metamagnetic transition at the critical point (T_3, H_3). As described in Sec. III, there is a first-order transition line between the AF phase and the P phase [see Fig. 1(b)]. This line persists up to the critical point (T_3, H_3) from T = 0 K, and joins smoothly on to a second-order line. On the first-order transition line, the magnetization M discontinuously changes from 0 to the saturation magnetization M_s corresponding to that of the ferromagnetic phase. In real systems, because of the geometry the internal magnetic field H_i is no longer equal to the external magnetic field H,[8] and is given by Eq. (5). The demagnetizing effects open the coexistence line into a coexistence area of AF and P phases [the (AF+P) phase] for the corresponding plot in the (T-H) plane, where the two phases coexist in varying proportions [see Fig. 1(c)]. As shown in Fig. 9(a) for a stage-1 $CoCl_2$ GIC, line H_{c4} is the boundary between the AF phase and (AF+P) phase and line H_{c5} is the boundary between the (AF+P) phase and the P phase. The values of H_{c4} and H_{c5} are described by $H_{c4}=H_E'$ and $H_{c5}=H_E'+N\Delta M_s$, where $\Delta M_s=\Delta M_a\rho_m/W$, ΔM_a (in units of emu/Co mol) is the change of the measured magnetization at T between lines H_{c4} and H_{c5}, ρ_m (=2.06 g/cm^3) is the density, and W (=197.46 g/Co mol) is the gram weight of the system per Co mole. Experimentally we have $H_{c4}\approx 350$ Oe and $H_{c5}\approx 1000$ Oe at $T=6$ K. From Fig. 6(a) we have $M_a=9788$ (emu/Co mol) at H_{c5} and $M_a=4320$ (emu/Co mol) at H_{c4} for $T=6$ K, leading to $\Delta M_a=5468$ (emu/Co mol) or $\Delta M_s=57.0$ emu/cm^3. Then the demagnetization factor can be estimated as $N=11.4$ ($N/4\pi=0.9$), which is much larger than that predicted from the geometry of the sample. Such a large N is partly due to the fact that our sample is highly nonellipsoidal in shape, thus giving rise to a large distribution in internal fields.

From Fig. 9(a) we find $H_{c4}=375$ Oe at $T=4.5$ K, indicating that $H_E'\approx 375$ Oe. This value of H_E' is in good agreement with that ($H_E'=380$ Oe) reported by Nicholls and Dresselhaus.[3] Using Eq. (6) with $H_E'=375$ Oe and H_2

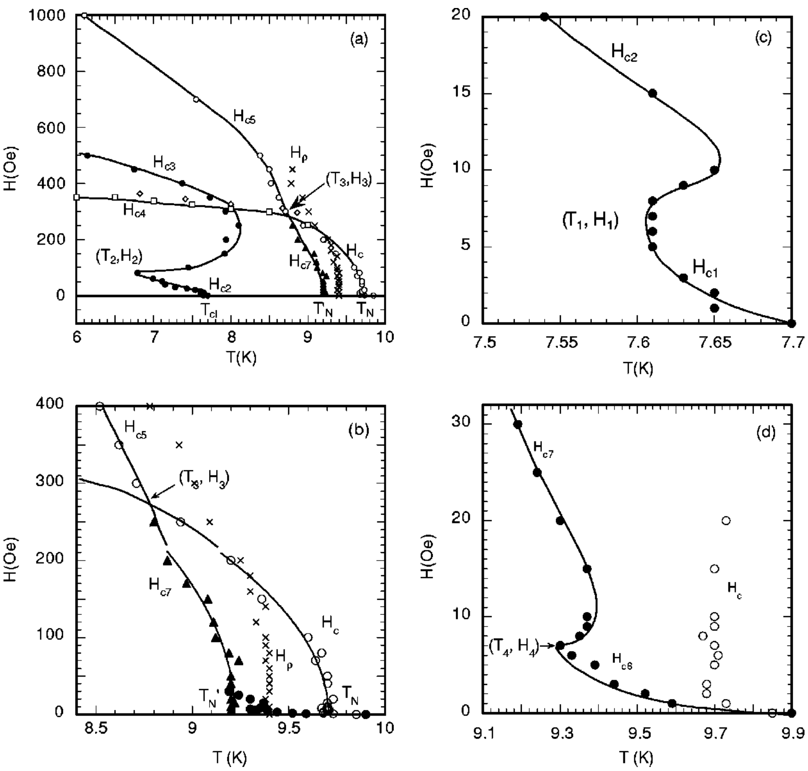

FIG. 9. (a) H-T diagram related to the metamagnetic transition at the critical point (T_3,H_3) and the spin-flop transition at the critical point (T_2,H_2). The data denoted by open diamonds are taken from Nicholls and Dresselhaus (Ref. 3). The solid lines are guides to the eye. (b) H-T diagram near T_N below 400 Oe. Lines H_c, H_{c5}, and H_{c7} are the phase boundaries. On line H_ρ $(\times)$, $d(\rho/\rho_0)/dT$ shows an anomaly. The solid lines at low H are the least-squares fits of the data to Eq. (7). $T_N=9.9$ K and $T_N'=9.25$ K. (c) H-T diagram near T_{cl} below 20 Oe. Lines H_{c1} and H_{c2} are the phase boundaries. The coordinate (T_1, H_1) is a critical point. (d) H-T diagram near T_N below 32 Oe. The lines H_c, H_{c6}, and H_{c7} are the phase boundaries. The coordinate (T_4,H_4) is a critical point.

$=80$ Oe, we obtain $J'=2.7\times10^{-2}$ K and $H_A^{in}=8.5$ Oe. The ratio J'/J is calculated as 3.5×10^{-3}, which is much larger than that $(J'/J=1.8\times10^{-4})$ for a stage-2 $CoCl_2$ GIC, where $J=7.75$ K and $J'=1.40\times10^{-3}$ K. In Figs. 9(a) and 9(b) we make a plot of the peak temperature of $d(\rho/\rho_0)/dT$ vs T for each H, showing a line denoted by H_ρ. This line is located near line H_{c7} below H_3 and near line H_{c5} above H_3. As shown in Fig. 7(a), the resistivity ρ for $H<H_3$ shows no hysteresis on crossing line H_ρ. The value of ρ measured with increasing T is the same as that with decreasing T. In contrast, the resistivity ρ for $350\leqslant H\leqslant 700$ Oe shows a hysteresis on crossing line H_ρ. The value of ρ measured with increasing T is larger than that with decreasing T. This result suggests that the transition in line H_ρ is of first order at least for $350\leqslant H\leqslant 700$ Oe.

In Fig. 9(b) we show the T dependence of lines H_c and H_{c7}. The dispersion χ' shows a maximum on crossing line H_c and dM_{FC}/dT has a local maximum on crossing line H_{c7}. The T dependence of lines H_c and H_{c7} is described by[20]

$$H^2=\alpha(T_c-T), \tag{7}$$

with $\alpha=(7.87\pm0.02)\times10^4$ (Oe^2/K) and $T_c=9.71\pm0.05$ K $(\approx T_N)$ for line H_c $(8.9\leqslant T\leqslant 9.7$ K) and $\alpha=(1.13\pm0.03)\times10^5$ (Oe^2/K) and $T_c=9.25\pm0.03$ K $(=T_N')$ for line H_{c7} $(8.4\leqslant T\leqslant 9.3$ K). For convenience T_N' is defined as a temperature where line H_{c7} intersects with the T axis. Note that line H_{c7} may correspond to a line observed in $FeBr_2$ which results from a decomposition of the tricritical point into a critical end point and a bicritical end point.[10–14] The corresponding line in $FeBr_2$ is of first order, while line H_{c7} in a stage-1 $CoCl_2$ GIC may be of second order. At present, the nature of the phase between lines H_c and H_{c7} is not clear.

We also note that the spin-flop transition at the critical point (T_3,H_3) in a stage-1 $CoCl_2$ GIC is similar to that in $FeCl_2$ $(T_N=23.6$ K) at the tricritical point $(T_t=21.15$ K, $H_t=10.2$ kOe),[8,9] where H is applied along the c axis. The ratio T_3/T_N $(=0.869)$ for a stage-1 $CoCl_2$ GIC is nearly equal to the ratio T_t/T_N $(=0.896)$ for $FeCl_2$. The only difference is the spin symmetry: XY-like for a stage-1 $CoCl_2$ GIC, and Ising-like for $FeCl_2$. In a layer of Fe^{2+} ions in $FeCl_2$ all spins lie parallel to each other and normal to the layer.

C. Other field-induced transitions

As shown in Figs. 9(c) and 9(d), we find two spin-flop transitions at critical points $(T_1\approx7.6$ K, $H_1\approx7$ Oe) and $(T_4=9.3$ K, $H_4=7$ Oe). The origin of the transition at (T_4,H_4) is not clear at present. Here we discuss only the nature of the spin-flop transition at the critical point (T_1, H_1). The lines H_{c1} and H_{c2} meet at the critical point. Since H_{c2} is much lower than $2H_E'$ and H_1 is lower than H_A^{in}, the fields H_E' and H_A^{in} do not contribute to this transition. One possibility is that this transition may be associated with that of a stage-2 $CoCl_2$ GIC which is contained as a minor phase. In fact, as shown in Figs. 6(b) and 8, the derivative dM_{ZFC}/dH shows a small sharp peak at low H for $T\leqslant7$ K: typically $H=15$ Oe at $T=4.5$ K. It is believed that such a transition at low H is due to the stage-2 contribution.[3] We assume that the spin-flop transition may be caused by the competition between an antiferromagnetic interplanar interaction field H_E'' and an in-plane anisotropic field $(H_A^{in})'$ for a stage-2 $CoCl_2$ GIC. Then the critical field H_1 and field H_{c2} are described by $H_1=\{[2H_E''-(H_A^{in})'](H_A^{in})'\}^{1/2}$ and $H_{c2}=2H_E''-(H_A^{in})'$. If $H_1=7$ Oe and $H_{c2}\approx20$ Oe, we obtain

$H''_E = 11.2$ Oe and $(H_A^{in})' = 2.45$ Oe. The characteristic field $(H_A^{in})'$ for the stage-2 system is relatively lower than H_A^{in} for the stage-1 system. We note that the ratio H''_E/H'_E is equal to 0.03, where H''_E is related to an antiferromagnetic interplanar interaction J'' through $H''_E = 2z'J''S/(g_a\mu_B)$. Then the ratio J''/J can be calculated as 1.03×10^{-4}, which is on the same order as that for the stage-2 $CoCl_2$ GIC. As shown in Fig. 8, we find anomalies in χ' and dM_{FC}/dT around $T=8.4$ K and $H\approx0$ in the $(T,\ H)$ plane: (i) the peak of χ' vs T for $8.25 \leqslant T \leqslant 8.5$ K and $5 \leqslant H \leqslant 20$ Oe, and (ii) the local minimum of dM_{FC}/dT vs T for $8.2 < T < 8.65$ K and $5 \leqslant H \leqslant 100$ Oe. Such anomalies are also due to the contribution from a stage-2 $CoCl_2$ GIC. In fact, the dispersion χ' of a stage-2 $CoCl_2$ GIC at $f=1$ Hz has a peak at 8.40 K in the absence of H.[21]

D. Nature of the low-temperature phase below T_{cl}

It is interesting to compare the critical temperatures of a stage-1 $CoCl_2$ GIC with those of a stage-2 $CoCl_2$ GIC. It is known that a stage-2 $CoCl_2$ GIC magnetically behaves like a quasi-2D XY ferromagnet with an extremely weak antiferromagnetic interplanar exchange interaction. This compound undergoes two magnetic phase transitions at T_{cu} and T_{cl}. These two critical temperatures are identified as peak temperatures of χ'' with $f=1$ Hz at $H=0$: $T_{cu}=8.9$ K and $T_{cl}=6.9$ K.[21] We find a noticeable increase in T_{cu} and T_{cl} as the stage number decreases from stage 2 to stage 1. The magnitude of antiferromagnetic interplanar interactions drastically increases as a result of the reduction of the c-axis repeat distance from 12.73 to 9.38 Å, leading to the change of dimension of the system from 2D-like to 3D-like. We note that the ratio T_{cu}/T_{cl} $(=1.286)$ for a stage-1 $CoCl_2$ GIC is almost the same as that $(=1.290)$ for a stage-2 $CoCl_2$ GIC, where T_{cu} $(=T_N=9.9$ K) and $T_{cl}=7.7$ K for a stage-1 $CoCl_2$ GIC. The ratio of T_{cu} of a stage-1 GIC to T_{cu} of a stage-2 GIC $(=1.112)$ is almost the same as the ratio of T_{cl} of a stage-1 GIC to T_{cl} of a stage-2 GIC $(=1.116)$. These results may suggest that the mechanism of spin ordering at $H=0$ is similar between stage-1 and stage-2 $CoCl_2$ GIC's.

Nevertheless, the spin order in a stage-1 $CoCl_2$ GIC is rather different from that in a stage-2 $CoCl_2$ GIC. In a stage-2 $CoCl_2$ GIC, the antiferromagnetic long-range spin order is established below T_{cl}, while in a stage-1 $CoCl_2$ GIC the 3D antiferromagnetic spin order is already established below T_N. What is the nature of the low-temperature phase below T_{cl} in stage-1 $CoCl_2$ GIC? Since H_A^{in} plays an important role for the spin-flop transition at (T_2,H_2), it is expected that the spin structure at $H=0$ below T_{cl} arises from the competition between H'_E and H_A^{in}. This problem is reduced to the 1D antiferromagnetic XY chain with in-plane sixfold anisotropy. When H_A^{in} is much smaller than H'_E, an usual AF state is energetically favorable. However, when H_A^{in} is not negligibly small compared to H'_E, the ordered phase is different from the usual AF phase. In fact, the spin structure as a function of the ratio H_A^{in}/H'_E can be determined from the minimum condition of the Landau free energy derived by Szeto and Dresselhaus.[17]

VII. CONCLUSION

We have determined the H-T diagram of a stage-1 $CoCl_2$ GIC. Because of extremely weak antiferromagnetic interplanar exchange interactions the entire H-T phase diagram is accessible below 2 kOe. The H-T diagram includes a metamagnetic transition and several spin-flop transitions, which arise from competitions between antiferromagnetic interplanar interactions and in-plane anisotropic interactions. The H-T diagram at very low H is complicated by the possible existence of a stage-2 $CoCl_2$ GIC as a minority phase. In order to obtain a deeper understanding of the H-T diagram of a stage-1 $CoCl_2$ GIC, a determination of spin structures is required using neutron-scattering experiments in the presence of H along the c plane.

ACKNOWLEDGMENTS

We would like to thank H. Suematsu for providing us with a single crystal of kish graphites. This work was partly supported by the Research Foundation at SUNY-Binghamton (240-9522A).

*Email address: itsuko@binghamton.edu
†Email address: suzuki@binghamton.edu

[1] D. G. Wiesler, M. Suzuki, P. C. Chow, and H. Zabel, Phys. Rev. B **34**, 7951 (1986).
[2] K. Y. Szeto, S. T. Chen, and G. Dresselhaus, Phys. Rev. B **33**, 3453 (1986).
[3] J. T. Nicholls and G. Dresselhaus, J. Phys.: Condens. Matter **2**, 8391 (1990).
[4] R. Yazami and G. Chouteau, Synth. Met. **18**, 543 (1987).
[5] H. Ikeda, Y. Endoh, and S. Mitsuda, J. Phys. Soc. Jpn. **54**, 3232 (1985).
[6] G. Chouteau, J. Schweizer, F. Tasset, and R. Yazami, Synth. Met. **23**, 249 (1988).
[7] N.-C. Yeh, K. Sugihara, M. S. Dresselhaus, and G. Dresselhaus, Phys. Rev. B **40**, 622 (1989).
[8] R. J. Birgeneau, G. Shirane, M. Blume, and W. C. Koehler, Phys. Rev. Lett. **33**, 1098 (1974).
[9] J. F. Dillon, Jr., E. Yi. Chen, and H. J. Guggenheim, Phys. Rev. B **18**, 377 (1978).
[10] M. M. P. de Azevedo, Ch. Binek, J. Kushauer, W. Kleemann, and D. Bertrand, J. Magn. Magn. Mater. **140**, 1557 (1995).
[11] H. Aruga Katori, K. Katsumata, and M. Katori, Phys. Rev. B **54**, R9620 (1996).
[12] K. Katsumata, H. Aruga Katori, S. M. Shapiro, and G. Shirane, Phys. Rev. B **55**, 11 466 (1997).
[13] O. Petracic, Ch. Binek, W. Kleemann, U. Neuhausen, and H. Lueken, Phys. Rev. B **57**, R11051 (1998).
[14] Ch. Binek, T. Kato, W. Kleemann, O. Petracic, D. Bertrand, F. Bourdarot, P. Burlet, H. Aruga Katori, K. Katsumata, K. Prokes, and S. Welzel, Eur. Phys. J. B **15**, 35 (2000).

[15] G. Dresselhaus, J. T. Nicholls, and M. S. Dresselhaus, in *Graphite Intercalation Compounds II*, edited by H. Zabel and S. A. Solin (Springer-Verlag, Berlin, 1990), p. 247.
[16] M. Suzuki, Crit. Rev. Solid State Mater. Sci. **16**, 237 (1990).
[17] K. Y. Szeto and G. Dresselhaus, Phys. Rev. B **32**, 3186 (1985).
[18] K. Yosida, *Theory of Magnetism* (Springer-Verlag, Berlin, 1996).
[19] A. H. Morrish, *The Physical Principles of Magnetism* (Wiley, New York, 1965).
[20] Y. Shapira and S. Foner, Phys. Rev. B **1**, 3083 (1970).
[21] M. Suzuki and I. S. Suzuki, Phys. Rev. B **58**, 840 (1998).